Atmospheric Research 247 (2021) 105145

Contents lists available at ScienceDirect

Atmospheric Research

journal homepage: www.elsevier.com/locate/atmosres

# Day–night variation and size distribution of water-soluble inorganic ions in particulate matter in Ulsan, South Korea

Tien Van Do, Quang Tran Vuong, Sung-Deuk Choi*

*School of Urban and Environmental Engineering, Ulsan National Institute of Science and Technology (UNIST), Ulsan, 44919, Republic of Korea*

ARTICLE INFO

*Keywords:*
Ion
Day–night variation
Size distribution
Particulate matter
Ulsan

ABSTRACT

In the present study, 11 size classes of particulate matter were collected from a semi-rural site in the industrial city of Ulsan, South Korea in 2019 to investigate the size distribution and day–night variation of water-soluble inorganic ions (WSIIs). Approximately 70% of the detected WSIIs were found in fine particles, with $Na^+$, $Ca^{2+}$, $Cl^-$, and $NO_3^-$ dominant (~70%) in coarse particles and $SO_4^{2-}$, $NO_3^-$, and $NH_4^+$ (SNA) dominant (~70%) in fine particles. Monthly variation in total WSIIs was observed, with the highest average concentration found in April for both coarse (2.71 μg/m$^3$) and fine particles (5.75 μg/m$^3$). Given that this month is characterized by prevailing southeasterly winds, these high levels may represent the adverse effects of industrial activity. Coefficients of divergence for individual WSIIs exhibited large variability, which is indicative of significant day–night differences in meteorology, chemistry, and source contributions. The size distributions of $Na^+$, $K^+$, $F^-$, $Cl^-$, $NO_3^-$, and $SO_4^{2-}$ were bimodal, while $Mg^{2+}$, $Ca^{2+}$, and $NH_4^+$ were unimodal. Peaks were generally found at 1.8–5.6 μm and 0.18–0.56 μm for coarse and fine particles, respectively. By plotting the linear relationship between the mole charge ratios of SNA, we found that coarse $NO_3^-$ particles were mainly the result of heterogeneous reactions between $HNO_3$ and sea salts or crustal species, while the homogeneous reaction of $HNO_3$ and $NH_3$ played a crucial role in the formation of fine $NO_3^-$ particles. In conclusion, though day–night variation in WSIIs was apparent, especially in SNA, the formation pathways for both coarse and fine particles were similar for day and night. Based on the verification of the formation mechanisms for WSIIs at this semi-rural site, the influence of industrial activity on the secondary formation of PM in urban and industrial areas can be investigated further.

## 1. Introduction

Recently, because of rapid economic growth and the increasing speed of urbanization and industrialization, particulate matter (PM) pollution has emerged as a serious environmental issue in Northeast Asia (Byun and Choi 2019; Kwon et al. 2019; Xing et al. 2020; Xu et al. 2020). PM has many damaging effects, such as reducing visibility, scattering and absorbing solar radiation, and infiltrating the lungs through inhalation, thus endangering human health (Kang et al. 2013; Tie and Cao 2009; Zhang et al. 2015). Aerosol particles, especially fine particles ($PM_{2.5}$, i.e., PM with 2.5 μm or less in aerodynamic diameter, $d_a$), can be derived from both primary sources, in which they are directly emitted from anthropogenic activity (e.g., vehicles, construction, and industry) into the atmosphere, and secondary aerosol formation, which involves gas condensation, heterogeneous reactions between particles, and in-cloud processes (Chan and Yao 2008; Matsuki et al. 2005; Shi et al. 2014; Sun et al. 2006).

The negative impact of PM depends on the characteristics of the aerosols, such as their size distribution, physical properties, and chemical composition. PM is a complex mixture of many chemical compounds (e.g., elemental species and carbonaceous species). Of these species, water-soluble inorganic ions (WSIIs), especially sulfate ($SO_4^{2-}$), nitrate ($NO_3^-$), and ammonium ($NH_4^+$), which are collectively referred to as SNA, are generally reported to be the dominant ionic species in $PM_{2.5}$, accounting for 60–70% of the total mass concentration (Ali-Mohamed 1991; Guo et al. 2014; Huang et al. 2014; Liu et al. 2018). SNA is mainly detected as ammonium salts such as $NH_4NO_3$ and $(NH_4)_2SO_4$ that form through the neutralization of ammonia ($NH_3$) and acidic species such as nitric acid ($HNO_3$) and sulfuric acid ($H_2SO_4$) (Squizzato et al. 2013; Stockwell et al. 2003). In addition, in coastal areas with high levels of sodium chloride (NaCl), sodium nitrate ($NaNO_3$) can be generated in the reaction between NaCl and $HNO_3$ (Eldering et al. 1991; Hu et al. 2008), while the reaction between $NH_3$ and hydrochloric acid (HCl) can produce ammonium chloride

* Corresponding author.
*E-mail address:* sdchoi@unist.ac.kr (S.-D. Choi).

https://doi.org/10.1016/j.atmosres.2020.105145
Received 24 May 2020; Received in revised form 7 July 2020; Accepted 16 July 2020
Available online 18 July 2020
0169-8095/ 

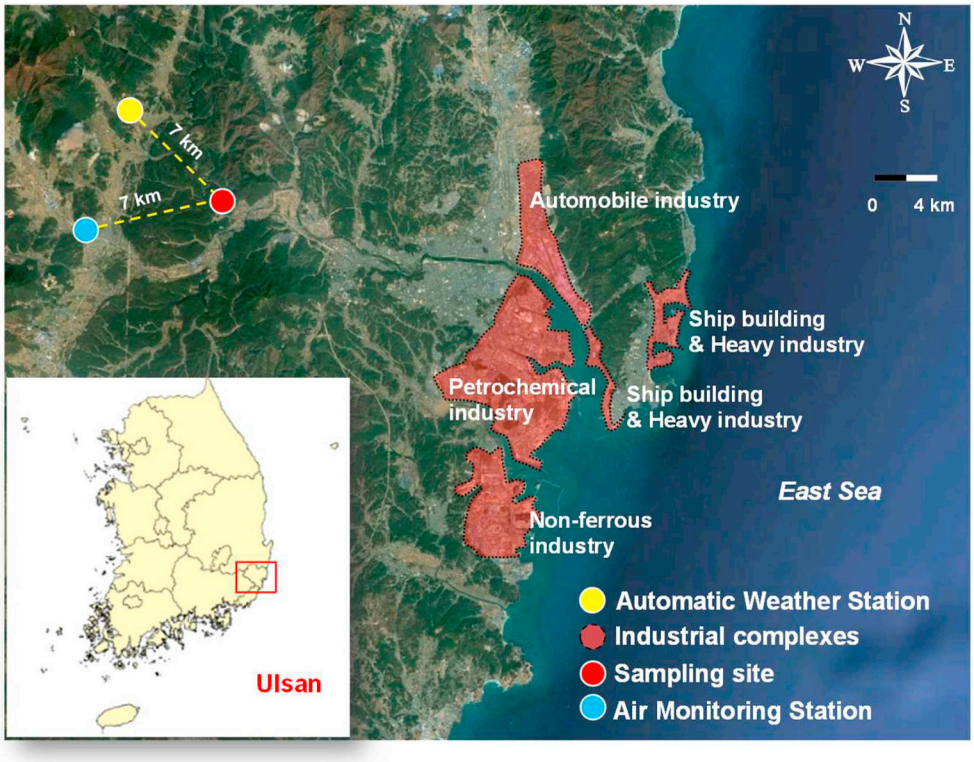


**Fig. 1.** Locations of the air monitoring station, automatic weather station, sampling site, and four major industrial complexes in Ulsan, South Korea. The yellow dashed line illustrates the distance between the air monitoring station or automatic weather station and the sampling site.

($NH_4Cl$) (Matsumoto and Okita 1998; Walker et al. 2006).

Previous research has reported that SNA, the dominant component of secondary inorganic aerosols (SIA), plays a crucial role in the generation of haze and reduces visibility during serious pollution episodes (Sudheer et al. 2014; Sun et al. 2004; Tian et al. 2016). The characteristics of atmospheric aerosols, including their formation mechanisms and potential sources, can be investigated based on their chemical composition and size distribution in relation to weather conditions and local emission sources (Contini et al. 2014; Xiu et al. 2004). Some studies have proposed that there are three dominant aerosol size modes – Aitken nuclei mode ($d_a$ < 0.1 μm), accumulation mode ($d_a$ = 0.1–2 μm), and coarse mode ($d_a$ > 2 μm) (Xiu et al. 2004; Zhang et al. 2018) – but that the size distribution varies under different conditions (Huang et al. 2016; Sun et al. 2013). Many studies have emphasized the complexity of SIA formation and have recommended further in-depth investigation, especially regarding the formation mechanisms for variously sized SIA particles. In recent years, although the ionic composition of coarse and fine particle fractions in South Korea has been reported (Kim et al. 2006; Park et al. 2016; Shon et al. 2012; Song et al. 2017), few studies have investigated the aerosol size distribution of WSIIs in South Korea (Park and Lee 2015; Park et al. 2019; Park et al. 2004). Furthermore, most previous research in South Korea has involved short-term measurements and focused on urban areas such as Seoul and Busan (Kim et al. 2006; Shon et al. 2012) or background areas such as Jeju Island and Baengnyeong Island (Kim et al. 1998; Lee et al. 2015).

Ulsan, the largest industrial city in South Korea, contains automobile, photochemical, non-ferrous, shipbuilding, and heavy industries. The influence of industrial activity on aerosol formation via the emission of massive volumes of gaseous precursors (e.g., $SO_2$ and $NO_2$) into the atmosphere has been reported (Clarke et al. 2014; Wu et al. 2009). In particular, $SO_2$ emissions from the petrochemical and non-ferrous industries in Ulsan have been found to have a significant impact on surrounding areas, while combustion associated with the energy industry, manufacturing combustion, transportation, and non-road mobile sources have been identified as sources of $NO_2$ in this study area (Clarke et al. 2014). Ulsan also has a long eastern coastal line that is strongly influenced by sea spray and meteorological conditions such as low temperatures during winter, characteristics that promote aerosol formation. However, few studies have characterized the ionic components of $PM_{2.5}$ and $PM_{10}$ in Ulsan (Park et al. 2019), nor have day–night differences in ionic composition been investigated. Therefore, a comprehensive analysis of the day–night difference and size distribution of WSIIs in Ulsan is necessary.

In this study, 11 different size classes of aerosol particles were collected from a semi-rural site in Ulsan, South Korea from January to November 2019 to better understand day–night variation in the ionic composition and size distribution of WSIIs. Meteorological data were also obtained to investigate their association with the ionic composition of both fine and coarse particles. From this analysis, the potential sources and formation mechanisms for the WSIIs found in the study area were identified. To date, this study represents the first comprehensive analysis of day–night variation in the ionic composition of individual WSII size groups in South Korea.

## 2. Materials and methods

### 2.1. Collection of size-segregated aerosol particles

Atmospheric aerosol samples were collected ($n$ = 572) on January 21–28, April 15–22, September 16–21, and November 11–18, 2019 both during the day (from 6:00 AM to 5:30 PM) and at night (from 6:00 PM on the first day to 5:30 AM the following day). A Micro-Orifice Uniform Deposit Impactor (120 MOUDI-II™, MSP Corp., USA) was installed on the rooftop of a three-story building at the Ulsan National Institute of Science and Technology (UNIST; 35°33′37.15″N, 129°22′15.76″E; 47 m above sea level), which is about 15 m above ground level (Fig. 1). The MOUDI sampler was operated with a flow

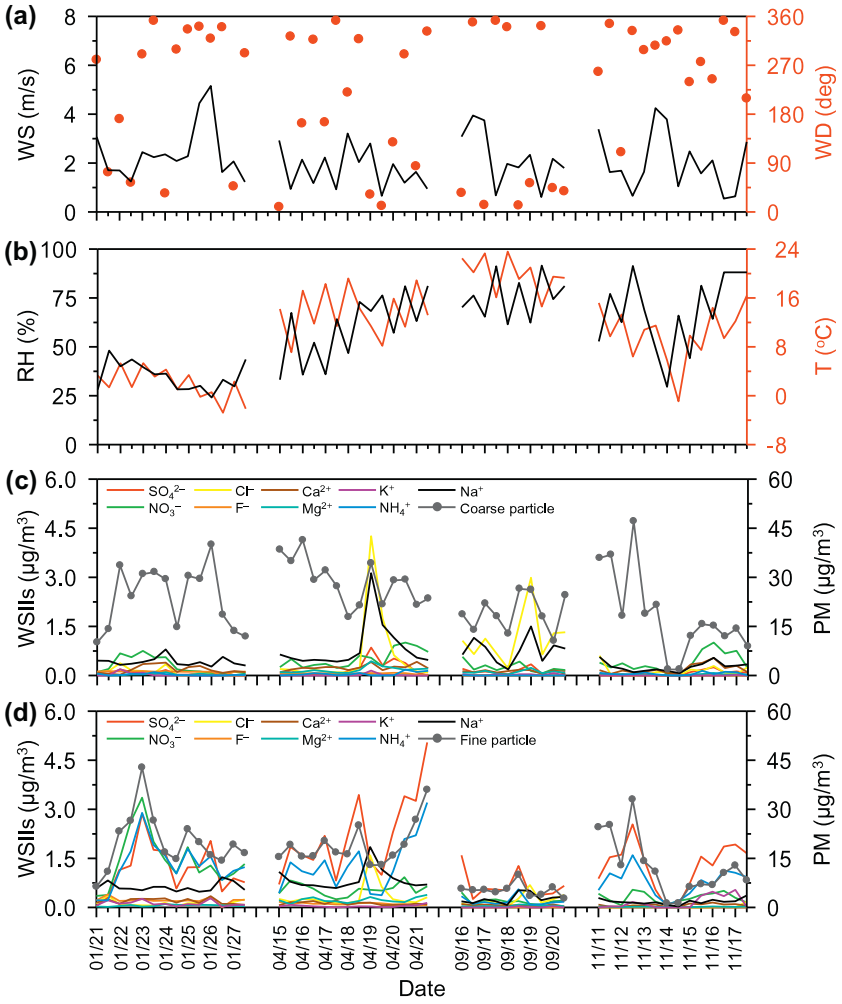


**Fig. 2.** Daily variation in the (a) wind direction (WD) and wind speed (WS), (b) temperature (T) and relative humidity (RH), and nine WSIIs detected in (c) coarse (1.8–18 μm) and (d) fine (0.056–1.8 μm) particles in 2019. The major and minor ticks on the x-axis represent the day and night, respectively.

rate of 30 L/min and 11 cut sizes (18.0, 10.0, 5.60, 3.20, 1.80, 1.00, 0.56, 0.32, 0.18, 0.10, and 0.056 μm). Aluminum foil filters (47 mm, TSI Incorporation, USA) were used to collect the atmospheric aerosol particles. To measure the PM concentration, all aluminum foil filters were stored in a controlled chamber (25 ± 1 °C and 40 ± 5% relative humidity) for 24 h and then weighed three times using a microbalance (MSE 3.6P–000–DM, Sartorius Weighing Technology GmbH, Germany) with a readability of $10^{-6}$ μg before and after sampling. The filters were intermediately transported back to the laboratory and stored at −20 °C prior to pretreatment and analysis.

### 2.2. Meteorological conditions and gaseous precursor data

Hourly meteorological data, including precipitation, wind direction, wind speed, relative humidity, and temperature were obtained from an automatic weather station (35°37′13.08″N, 129°8′36.60″E) operated by the Korea Meteorological Administration (KMA, https://data.kma.go.kr). A summary of the meteorological data is provided in Table S1 in the Supplementary Information. The temperature was highest (23.6 °C) in September and lowest (−2.78 °C) in January, with an average temperature over the entire sampling period of 11.4 °C. The wind was generally stronger during the day than during the night, with northwesterly winds in January and November, southeasterly winds in April, and northeasterly winds in September (Fig. S1). Because sampling was conducted to avoid specific meteorological events, e.g., rain and snow, precipitation was not a confounding factor during the sampling period. The average relative humidity was 51.8% and 67.5% during the day and at night, respectively. More detailed information on the meteorological conditions during the sampling period is presented in Table S1.

Gaseous precursor data ($SO_2$ and $NO_2$) were also obtained at an air monitoring station (Samnam, 35°33′29.41″N, 129°6′49.54″E) in Ulsan (Fig. 1) via the Air Korea website (https://www.airkorea.or.kr).

### 2.3. Analysis of WSIIs and QA/QC

Each filter was transferred into a 15-mL conical tube (high-clarity polypropylene, 17 mm in diameter × 120 mm in length, Falcon, Mexico). Deionized water (18.2 MΩ cm, 6 mL) was used for extraction for 45 min at room temperature in an ultrasonic bath (39 kHz). After extraction, a polytetrafluoroethylene single-use syringe filter (pore size 0.22 μm, Whatman, Germany) was used to filter the extract before instrumental analysis using an ion chromatography system (ICS–3000, Thermal Fisher Scientific Inc., USA). IONPAC CS17 (4 mm × 250 mm) and IONPAC AS16 (4 mm × 250 mm) analytical columns were employed in the analysis of five cations ($Ca^{2+}$, $Mg^{2+}$, $K^+$, $NH_4^+$, and $Na^+$) and four anions ($SO_4^{2-}$, $NO_3^-$, $Cl^-$, and $F^-$), respectively. Detailed specifications for the instruments used in ion analysis are reported in Table S2.

The standard calibration curves (range of 0.005–5 μg/mL) for individual ionic species had high coefficients of determination ($r^2$ > 0.995). Field blanks were regularly sampled for each batch ($n$ = 52). The pretreatment and analytical processes for the blank

samples were the same as those used for the real samples. The concentration of all real samples was then corrected using the blank samples (no greater than 0.004 μg/m$^3$). The recovery rates of the WSIIs (81–106%) were calculated by analyzing seven spiked samples of 0.01 μg/mL multi-component cation (IC–MCA–02–01, AccuStandard, Inc., USA) and anion (IC–MAN–10–R1–1, AccuStandard, Inc., USA) standards using the same process as for the real samples. The method detection limit (MDL) for the individual inorganic species was given by Eq. (1):

$$MDL = SD \times t_s \quad (1)$$

where SD is the standard deviation for seven replicates of the spiked samples, and $t_s$ is the Student's *t*-statistic (3.14) for a 99% confidence interval. The MDLs were 0.002, 0.003, 0.002, 0.006, 0.004, 0.020, 0.004, 0.020, and 0.003 μg/m$^3$ for $Ca^{2+}$, $Mg^{2+}$, $K^+$, $NH_4^+$, $Na^+$, $SO_4^{2-}$, $NO_3^-$, $Cl^-$, and $F^-$, respectively. Values below these MDLs were replaced with 1/2 MDL in the calculation of the mean.

### 2.4. Coefficient of divergence

The coefficient of divergence (COD), a self-normalizing parameter, was used to quantify day–night variation and was calculated as follows:

$$COD_{t_1t_2} = \sqrt{\frac{1}{P}\sum_{i=1}^{P}\left(\frac{x_{it_1}-x_{it_2}}{x_{it_1}+x_{it_2}}\right)^2} \quad (2)$$

where $x_{it_1}$ and $x_{it_2}$ are the average concentrations of component *i* at sampling times $t_1$ and $t_2$, respectively, and *P* is the number of observations (Wilson et al. 2005).

## 3. Results and discussion

### 3.1. Temporal variation in PM and WSIIs

#### 3.1.1. Daily variation in PM and WSIIs

Fig. 2 illustrates the daily variation in key meteorological parameters and the ionic composition of coarse and fine particles during the sampling period. In this study, because there was no cut-off at 2.5 μm in the MOUDI sampler, the cut size at 1.8 μm was used to separate the particles by size; particles with a $d_a$ smaller than 1.8 μm were classified as fine and those with a $d_a$ of 1.8–18 μm were classified as coarse. Daily mass concentrations of total WSIIs in coarse mode ranged from 0.17 to 9.86 μg/m$^3$ (average: 1.88 μg/m$^3$), thus accounting for 0.97–28.8% of the concentration of all coarse particles (1.84 to 47.2 μg/m$^3$; average: 22.8 μg/m$^3$) (Fig. 2c). During the sampling period, peaks for daily $Na^+$ (0.08–3.13 μg/m$^3$; average: 0.56 μg/m$^3$) and $Cl^-$ (0.02–4.26 μg/m$^3$; average: 0.45 μg/m$^3$) in the coarse particles were found on April 19–20, September 16–19, and November 11–12, which may be associated with the southeasterly winds generated by sea-breeze circulation (Fig. 2a). Other WSIIs did not exhibit any obvious peaks in coarse mode, and no significant correlations between WSIIs and coarse particles were found (Table S3).

For fine particles, the daily mass concentration of total WSIIs varied from 0.30 to 10.6 μg/m$^3$ (average: 4.04 μg/m$^3$) compared to a total concentration of 1.26 to 42.8 μg/m$^3$ (average: 14.9 μg/m$^3$), thus accounting for 9.22–67.2% (Fig. 2d). The positive correlations between fine particles and most WSIIs (Table S4) except for $Cl^-$ highlighted the crucial role of ionic composition in the formation of fine PM in the atmosphere. Daily $SO_4^{2-}$ in fine particles varied from 0.02 to 5.05 μg/m$^3$ (average: 1.37 μg/m$^3$), though there were noticeable peaks in each of the four months during the sampling campaign except in September. This is likely due to the influence of industrial sources in the vicinity that emit the gaseous precursor $SO_2$. It is obvious that northwesterly winds were dominant during all of fine $SO_4^{2-}$-peak days. In order to evaluate the influences of air pollutant transport by northwesterly winds, the relationships between fine $SO_4^{2-}$, WD, and WS are demonstrated in Fig. S2. In January, the higher concentrations of $SO_4^{2-}$ were related to higher WS of northwesterly winds (Fig. S2a), which indicates the crucial role of air pollutant transport. In contrast, the higher levels of $SO_4^{2-}$ in April and November were more associated with lower WS of northwesterly winds (Figs. S2b, c). Therefore, $SO_4^{2-}$ might originate from local sources because higher WS would normally dilute the pollutants. The daily concentration of fine $NO_3^-$ varied from 0.07–3.36 μg/m$^3$ (average: 0.65 μg/m$^3$) and had a negative correlation with temperature ($r = -0.595$, $p < 0.01$), which could be explained by the temperature-dependent equilibrium of $NH_4NO_3$ (discussed in more detail in Section 3.1.2). Thus, the only obvious peak in fine $NO_3^-$ was observed in January. Daily $NH_4^+$ levels varied from 0.08–3.21 μg/m$^3$ (average: 0.95 μg/m$^3$) and tracked $NO_3^-$ ($r = 0.761$, $p < 0.01$) and $SO_4^{2-}$ ($r = 0.824$, $p < 0.01$) levels closely in fine mode, which explains the presence of $NH_4NO_3$ and/or $(NH_4)_2SO_4$ in fine particles. Other WSIIs varied by a factor of 100, which might be due to differences in the meteorological conditions (Figs. 2a, b) and potential sources over the four-month sampling period.

#### 3.1.2. Monthly variation in WSIIs

Monthly variation in the nine WSIIs and their fractions during the sampling campaign is presented in Fig. 3. Monthly variation in total fine WSIIs was evident (Fig. 3a), with the average concentration higher in January (5.29 μg/m$^3$) and April (5.75 μg/m$^3$) and lower in September (1.68 μg/m$^3$) and November (2.78 μg/m$^3$) (Table S5), accounting for 26.6%, 30.2%, 31.7%, and 22.2% of the fine particles, respectively. Approximately 70% of the WSIIs were found in fine

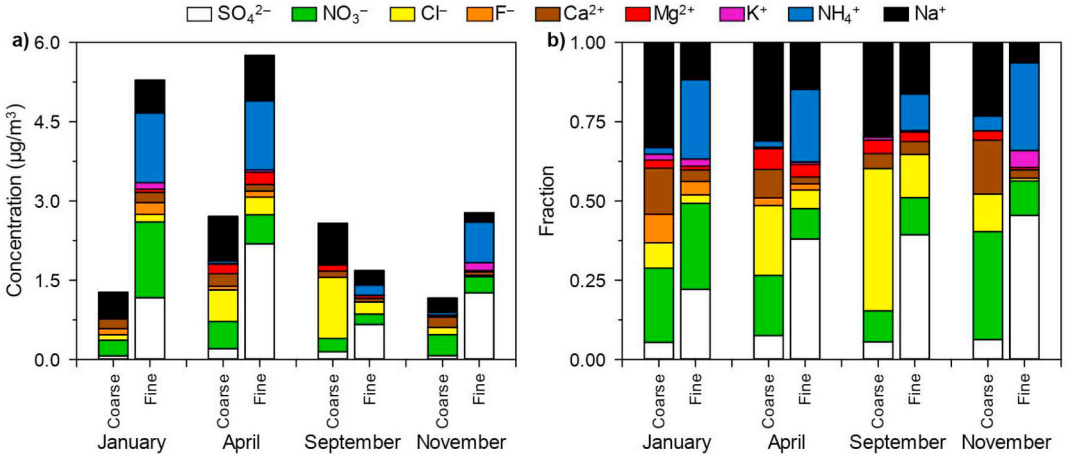


**Fig. 3.** Monthly variation in (a) nine WSIIs and (b) their fractions during the sampling period.

particles, with SNA the largest contributors, accounting for 50% of the total detected inorganic ions and about 70% of the total ionic species in fine mode (Fig. 3b).

$SO_4^{2-}$ is generally known to be mainly present in secondary fine particles formed through the chemical reaction of gaseous precursors (e.g., dimethyl sulfide and $SO_2$), including heterogeneous transformation processes (e.g., the $H_2O_2/O_3$ or metal-catalyzed oxidation of $SO_2$) and the homogeneous reaction between gaseous $SO_2$ and OH radicals (Meng et al. 2016; Zhou et al. 2016). Therefore, the dominance of $SO_4^{2-}$ in fine particles may be associated with high levels of $SO_2$ (average: 3.18, 4.10, 2.50, and 3.70 ppb in January, April, September, and November, respectively), and the peak in $SO_4^{2-}$ in April (2.19 μg/m$^3$) (Table S5) is likely due to the high temperature and relative solar radiation, which facilitate the transformation of the $SO_2$ emitted from industrial areas into $SO_4^{2-}$. In addition, the high RH in April (Fig. 2b) might favor the formation of fine $SO_4^{2-}$ through the aqueous or heterogenous transformation processes, which is related to the peak in $SO_4^{2-}$ in April. Although the concentrations of $SO_2$ in Ulsan have generally been reported to be highest during warm periods, especially during summer (Clarke et al. 2014), the average concentration of $SO_4^{2-}$ (0.66 μg/m$^3$) in fine mode was lowest in September (Table S5). This can be explained by the northeasterly winds in September (Fig. S1). As a rough comparison, the average level of $SO_4^{2-}$ found in this research was slightly higher than that observed at a residential site in Ulsan, while it was lower than that reported for other sites in South Korea (Table S6). This could be explained by the lower concentration of $SO_2$ at this semi-rural site compared to urban sites in Seoul, Daegu, and Busan and industrial sites in Ulsan. Most other studies conducted in South Korea have focused on very short-term measurements during significant events, such as periods of high PM pollution and/or Asian dust, making a direct comparison with the present study difficult (Table S6).

In fine mode, $SO_4^{2-}$ was found to be the dominant contributor in all months, while $NO_3^-$ and $NH_4^+$ were obviously higher during the cold periods. A negative correlation between temperature and both $NH_4^+$ ($r = -0.364$, $p < 0.01$) and $NO_3^-$ ($r = -0.595$, $p < 0.01$) in fine mode was observed (Table S4), indicating the volatilization of $NH_4NO_3$ under high temperatures. In addition, the average concentration of gaseous $NO_2$ was also found to be the highest in January (14.1 ppb) and the lowest in September (7.70 ppb). These could explain why the highest average concentration of $NH_4^+$ (1.32 μg/m$^3$) and $NO_3^-$ (1.43 μg/m$^3$) was in January and why the lowest (0.19 μg/m$^3$ and 0.20 μg/m$^3$, respectively) was in September ($p < 0.01$, Mann-Whitney rank sum test, Table S5). The presence of $NO_3^-$ in both fine and coarse particles has been reported in past research, while $NH_4^+$ and $SO_4^{2-}$ are mainly found in fine mode (Huang et al. 2016; Li et al. 2014; Zhang et al. 2018). Because of differences in the mechanisms underlying the formation of coarse and fine $NO_3^-$ particles, their size distribution is strongly associated with geographical location, meteorological conditions, and potential sources. A comprehensive discussion is presented later in this section.

$Na^+$ mainly originates from sea sources and was observed in fine particles across the entire sampling period, while $Cl^-$ in fine mode had a much higher average concentration in April (0.34 μg/m$^3$) and September (0.23 μg/m$^3$) than in January (0.14 μg/m$^3$) and November (0.02 μg/m$^3$) (Table S5). This may be the result of the transport on southeasterly winds of $Cl^-$ emitted from the industrial burning of coal (Fig. S1) (Yudovich and Ketris 2006). $K^+$ in fine mode is generally known as a marker of biomass burning events (Deshmukh et al. 2012; Zhao and Gao 2008); in the present study, it was highest in November (0.15 μg/m$^3$), followed by January (0.12 μg/m$^3$), April (0.04 μg/m$^3$), and September (0.01 μg/m$^3$) (Table S5).

The monthly variation in the ionic composition of coarse particles differed considerably to that observed for fine particles. The average concentration of total WSIIs was 1.27 μg/m$^3$, 2.71 μg/m$^3$, 2.58 μg/m$^3$, and 1.16 μg/m$^3$ (Fig. 3a) in January, April, September, and November, respectively, representing 5.34%, 9.44%, 13.5%, and 15.0% of all coarse particles. Of the nine detected WSIIs, $NO_3^-$, $Cl^-$, and $Na^+$ were dominant, accounting for up to 72.1% and 84.6% in April and September, respectively, while $Ca^{2+}$, $NO_3^-$, and $Na^+$ were largest contributors (~70%) to total WSIIs in coarse particles in January and November (Fig. 3b). Fine $NO_3^-$ is generated by the homogeneous reaction of gaseous $NH_3$ and $HNO_3$ shown in Reaction (1), whereas $NO_3^-$ in coarse particles can arise from the heterogeneous reaction between gaseous $HNO_3$ and sea-salt particles, as shown in Reaction (2) (Feng and Penner 2007; Ocskay et al. 2006).

$$HNO_{3\,(g)} + NH_{3\,(g)} \leftrightarrow NH_4NO_{3\,(s,aq)} \quad (1)$$

$$HNO_{3\,(g)} + NaCl_{\,(s)} \rightarrow NaNO_{3\,(s)} + HCl_{\,(g)} \quad (2)$$

$$NH_4NO_{3\,(s,aq)} + NaCl_{\,(s)} \rightarrow NaNO_{3\,(s)} + NH_4Cl_{\,(g)} \quad (3)$$

On hot summer days, $HNO_3$ does not easily react with $NH_3$ due to the reverse direction of Reaction (1). Previous studies have reported that $NH_4NO_3$ aerosols are not stable under low relative humidity and high temperatures (Mozurkewich 1993; Pio and Harrison 1987; Zhang et al. 2008). This can explain why the levels of fine $NO_3^-$ in winter were generally higher than in the other seasons. In addition, Ulsan is a coastal city; thus, sea-salt particles are expected to be the dominant coarse particle due to sea-breeze circulation. When the sea-salt concentration is sufficiently high, $HNO_3$ gas tends to react with NaCl to form $NaNO_3$ (Reaction 2), and $NaNO_3$ generally accumulates in particles with a size of 3.2–6.0 μm (Xiu et al. 2004).

$NO_3^-$ was found to be one of the most abundant species in coarse particles in April and September but was not detected in high quantities in fine particles. This suggests that, although $NH_4NO_3$ is volatile under high temperatures during warm periods, the formation of $NO_3^-$ in coarse particles via Reaction (2) might also be enhanced at high temperatures in April and September (Galindo and Yubero 2017; Zhang et al. 2018). This is consistent with our finding that $Na^+$ was more abundant than secondary aerosol species (i.e., SNA) in coarse mode, whereas SNA was dominant in fine particles. The concentration of $Na^+$ in coarse particles found in the present study is similar to that in reported for Busan, lower than that found in Jeju Island, and higher than the levels at most other sites (Table S6). The relatively low concentration of $NH_4^+$ in coarse particles could be explained by a negative artifact involving NaCl and $NH_4NO_3$ (Reaction 3) in the filters during sampling (Nicolás et al. 2009; Querol et al. 2004). This also suggests that $NH_4^+$ mainly accumulates in fine particles.

$Ca^{2+}$ was one of the dominant WSIIs in coarse mode in January (14.6%) and November (17.0%) (Fig. 3b), originating from falling dust and soil particles. Previous studies have found that marine and crustal species can react with gaseous $H_2SO_4$ and $HNO_3$ or their gaseous precursors on pre-existing coarse particles via heterogeneous condensation (Galindo and Yubero 2017). A positive correlation between $Ca^{2+}$ and both $NO_3^-$ ($r = 0.643$, $p < 0.01$) and $SO_4^{2-}$ ($r = 0.362$, $p < 0.01$) in coarse mode was observed (Table S3), suggesting that the high levels of coarse $Ca^{2+}$ can be explained by these reactions. The average concentration of $Cl^-$ was 0.10 μg/m$^3$, 0.60 μg/m$^3$, 1.16 μg/m$^3$, and 0.14 μg/m$^3$ in January, April, September, and November, respectively, accounting for 8.06%, 22.1%, 44.9%, and 11.8% of total WSIIs in coarse particles (Figs. 3a, b). The higher levels of $Cl^-$ in April and September than in January and November (Table S5) may possibly be due to marine sources from the East Sea (Fig. S1). $Mg^{2+}$ in coarse particles had a higher average concentration in April (0.24 μg/m$^3$) and September (0.11 μg/m$^3$) than in January (0.03 μg/m$^3$) and November (0.03 μg/m$^3$) (Table S5), which may be due to blowing and construction-derived dust. The concentration of $F^-$ in coarse particles was relatively low and did not exhibit any clear temporal patterns.

### 3.2. Day–night variation in WSIIs in fine and coarse particles

A summary of the average concentration of coarse and fine particle concentrations and their chemical composition during the day and at night over the sampling period is presented in Table S7. A statistically

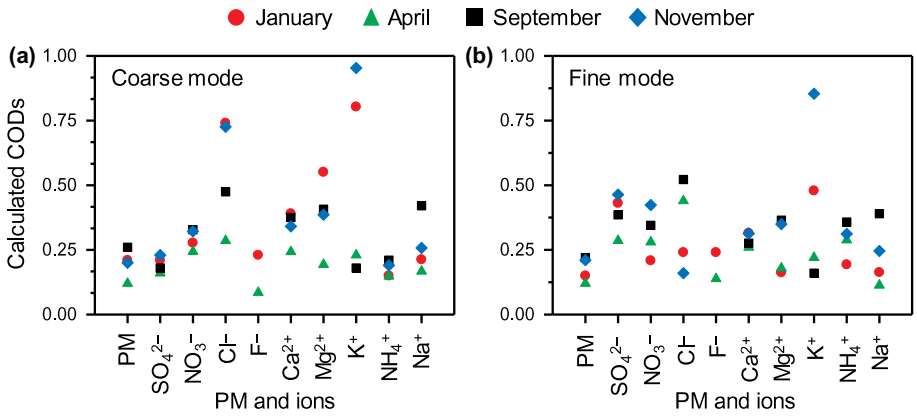


**Fig. 4.** COD analysis for day-time and night-time concentrations of nine WSIIs in (a) coarse and (b) fine particles during the four-month sampling period in Ulsan.

significant difference between day and night was only observed for $K^+$ in coarse mode in January ($p < 0.01$, Mann-Whitney rank sum test) and November ($p < 0.05$, Mann-Whitney rank sum test) with a higher average concentration during the day than at night (Table S7). This may be because dust sources are more influential during the day as a result of transportation and stronger wind patterns (Table S1).

The temporal variation in individual WSIIs between day and night was also assessed using the COD. The COD is a useful parameter for comparing the degree of uniformity among selected chemical components for both short- and long-term measurements (Li et al. 2013; Wongphatarakul et al. 1998; Yang et al. 2005). If there is no considerable difference between two sampling periods, the COD approaches zero. In contrast, a COD approaching unity is indicative of a significant difference between two sampling periods (Wang et al. 2005). A COD of 0.27 was used in this study to differentiate between homogeneity and heterogeneity for day–night in accordance with other studies (Chandra et al. 2019; Wilson et al. 2005).

Fig. 4 presents the monthly average COD for PM and the nine WSIIs in both coarse and fine mode during the sampling period. Generally, the COD in this study ranged from 0.09–0.95 and 0.11–0.85 for coarse and fine particles, respectively. The CODs were 0.21, 0.12, 0.26, and 0.20 for coarse PM and 0.15, 0.12, 0.22, and 0.21 for fine PM in January, April, September, and November, respectively, indicating that the PM sources during the day and night were similar. In terms of the WSIIs, the CODs exhibited large variability for both coarse and fine particles, suggesting that there were significant differences in meteorological conditions, chemistry, and source contributions between the day and night.

The calculated CODs for $Na^+$ in coarse particles were 0.21, 0.17, 0.42, and 0.26 in January, April, September, and November, respectively, which may be associated with the northeasterly winds during the day in September (Fig. S1). The higher average concentration of $Na^+$ during the day (0.82 μg/m$^3$) than at night (0.72 μg/m$^3$) in September may be due to the formation of $NaNO_3$ in coarse particles at high daytime temperatures (Galindo and Yubero 2017). This is consistent with our finding that the COD for $NO_3^-$ was higher than 0.27 in September (0.33), and November (0.32), with a higher average concentration during the day than at night (Table S7). The CODs of $Cl^-$ were higher than 0.27 (Fig. 4a), and the average concentrations of $Cl^-$ during the day were higher than those at night in all months (Table S7). This could be explained by differences in the prevailing winds during the day and at night over the sampling period, leading to greater marine source contributions to coarse particles during the day (Fig. S1). $SO_4^{2-}$, $F^-$, and $NH_4^+$, which were minor contributors to coarse mode, did not exhibit any obvious day–night differences, with relatively low CODs (Fig. 4a). The CODs of $Mg^{2+}$ and $Ca^{2+}$ were higher than 0.27 in all months except April, with a higher average concentration during the day (Table S7), possibly because soil particles and falling dust were more influential sources during the day due to the stronger winds (Table S1). $K^+$ in coarse mode had CODs of 0.80 and 0.95 in January and November, respectively, which again may be the result of dust sources being more influential during the day.

In fine particles, the COD of $SO_4^{2-}$ was consistently higher than 0.27 (Fig. 4b). The average concentration of fine $SO_4^{2-}$ during the day was higher at night in January and September (Table S7), which is likely to be associated with high levels of $SO_2$ and/or the stronger relative solar radiation/temperature during the day (Table S1). In contrast, the average concentration of fine $SO_4^{2-}$ was higher at night in April and November. This could be explained by large volumes of $SO_2$ being emitted from another source, such as short-range transport on northwesterly winds from areas surrounding Ulsan at night in April and November (Fig. S1). The CODs of $NO_3^-$ (0.21) and $NH_4^+$ (0.19) were only lower than 0.27 in January, possibly because the difference in meteorological conditions between day and night was smaller in January than in the other months (Table S1). The concentrations of fine $NH_4^+$ and $NO_3^-$ during the day were slightly lower than those at night in April, September, and November (Table S7), with the higher daytime temperatures enhancing the volatilization of $NH_4NO_3$ in fine particles. The CODs of $Cl^-$ in fine mode were 0.24, 0.44, 0.52, and 0.16 in January, April, September, and November, respectively, with an average concentration that was higher during the day than at night in April and September (Table S7). This could represent the influence of industrial sources that employ coal combustion during working hours. Indications of biomass burning were observed in January (COD = 0.48) and November (COD = 0.85), with a higher average concentration of $K^+$ in fine mode during the day than at night (Table S7). $Na^+$, $Mg^{2+}$, $Ca^{2+}$, and $F^-$ in fine particles showed patterns similar to those in coarse mode (Figs. 4a, b).

### 3.3. Size distribution of individual WSIIs

The potential sources and physicochemical properties of aerosols can be explained by the size distributions of their chemical components (Cabada et al. 2004; Contini et al. 2014; Liu et al. 2008). Fig. 5 illustrates the size distributions of nine WSIIs. In general, the size distributions of $Na^+$, $K^+$, $F^-$, $Cl^-$, $NO_3^-$, and $SO_4^{2-}$ were bimodal in nature, with fine particles peaking at 0.18–0.56 μm and coarse particles peaking at 1.8–5.6 μm. $NH_4^+$ was mainly found with peaks in the size range of 0.18–0.56 μm, thus demonstrating a unimodal distribution of fine particles. Similarly, both $Mg^{2+}$ and $Ca^{2+}$ were unimodal, peaking at 1.8–5.6 μm.

#### 3.3.1. Sulfate, nitrate, and ammonium

SNA, the most common SIA components, were found to be the dominant species, contributing up to 70% of the mass concentration of fine particles. In agreement with previous research (Huang et al. 2016;

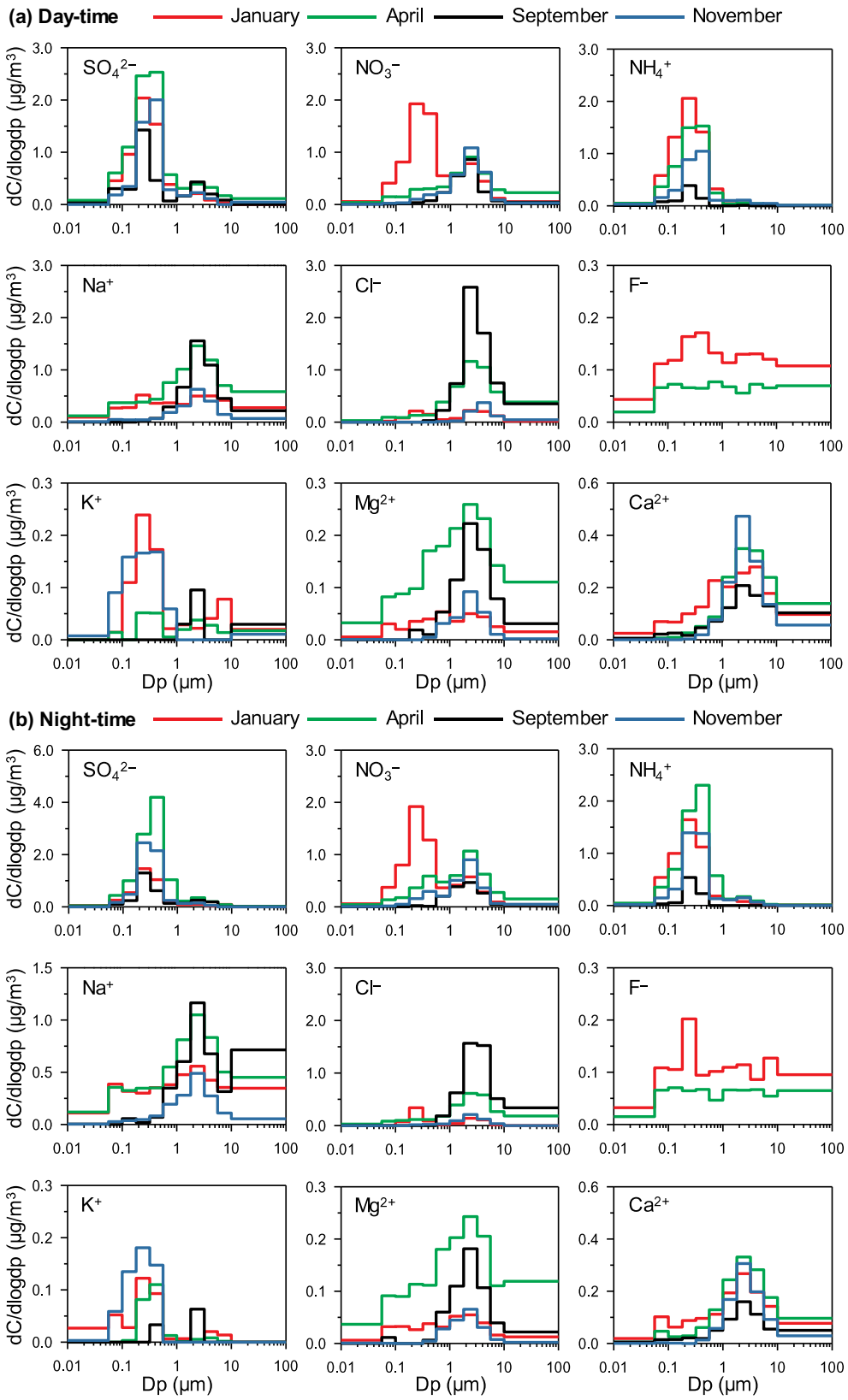


**Fig. 5.** Size distribution of nine WSIIs (a) during the day and (b) at night for the four sampling months. dC is the average concentration of the ions in each cut size. Dlogdp is the difference in the log between two consecutive cut sizes.

Zhao and Gao 2008), $SO_4^{2-}$ was detected primarily in fine mode, with peaks around 0.18–0.56 µm. $SO_4^{2-}$ is emitted from primary sources such as meat cooking and wood burning, accumulating in PM with a $d_a$ of 0.1 µm (Kleeman et al. 1999), and secondary processes via the oxidation of gaseous precursors to $H_2SO_4$ (Yamasoe et al. 2000). In the present study, $SO_4^{2-}$ within the 0.1–0.18 µm size range accounted for

20.0% and 17.3% of the $PM_{1.8}$ $SO_4^{2-}$ mass concentration during the day and at night, respectively. According to previous reports (Kleeman et al. 1999; Yamasoe et al. 2000), $K^+$ is known as an indicator of biomass burning, and the ratio of $K^+/SO_4^{2-}$ is close to 1 in fine mode when emitted from this source. In the present study, the average ratio of $K^+$ to $SO_4^{2-}$ was 0.12. 0.03, 0.04, and 0.14 during the day and 0.11, 0.02, 0.03, and 0.09 at night in January, April, September, and November, respectively, indicating that biomass combustion was not a major contributor to fine $SO_4^{2-}$. In addition, $SO_4^{2-}$ exhibited a small peak within the 3.2–5.6 μm size range in April, September, and November, which could be associated with sea salts and/or secondary $SO_4^{2-}$ generated in the reaction between $SO_2$ or $H_2SO_4$ and pre-existing $Ca^{2+}$ and/or $Na^+$ particles (Pakkanen 1996; Sievering et al. 1995). More detailed discussion of this is provided later in this section. A similar result, with two peaks in both coarse and fine particles, has been observed for $SO_4^{2-}$ in Ulsan, South Korea (Park et al. 2019).

As with $SO_4^{2-}$, the size distribution of $NH_4^+$ was unimodal, peaking at 0.18–0.56 μm with more than 95% found in fine particles. This indicates that gas-to-particle condensation reactions may be the dominant process in the formation of $NH_4^+$. Gaseous $NH_3$ in the atmosphere can neutralize $HNO_3$ and $H_2SO_4$ to form ammonium salts. At high $NH_3$ concentrations, $NH_4NO_3$ tends to form under high relative humidity and low temperatures, while the generation of $(NH_4)_2SO_4$ is favored at low $NH_3$ concentrations (Pathak et al. 2009a; Salvador et al. 2004a; Salvador et al. 2004b; Stockwell et al. 2000).

Of the SIA species, $NO_3^-$ exhibited an obvious day–night difference in size distribution across the entire sampling period. $NO_3^-$ had a bimodal distribution both during the day and at night in January, peaking at 0.18–0.56 μm and 3.2–5.6 μm in fine and coarse particles, respectively. This result is in direct accordance with previous studies conducted in South Korea (Park and Lee 2015; Park et al. 2019; Park et al. 2004). The peak in the fine particles may arise from gas-to-particle conversion, while that for coarse particles may be the result of the heterogeneous reaction between $HNO_3$ and crustal species or sea salts (Kawamura et al. 2007; Ocskay et al. 2006). During the day, $NO_3^-$ has a unimodal distribution in April, September, and November, peaking at 3.2–5.6 μm (Fig. 5a). This again is indicative of the temperature-dependent equilibrium of $NH_4NO_3$ in fine mode under high temperatures during the day in April, September, and November. The temperature is lower at night, which is beneficial for the generation of fine particulate $NO_3^-$ via gas-to-particle conversion. The loss of the fine $NO_3^-$ peak in September (Fig. 5b) may be because the highest temperatures of the sampling period occurred during this month, even at night. These findings agree closely with previous studies that have reported coarse $NO_3^-$ dominating during warm periods and fine $NO_3^-$ dominating during cold periods (Kadowaki 1976; Yoshizumi and Hoshi 1985).

The mole charge ratio of $[NH_4^+]$ to that of both $[SO_4^{2-}]$ and $[SO_4^{2-}]$ + $[NO_3^-]$ in coarse mode is presented in Fig. S3. Overall, 37.5% of the individual samples taken during the day had a $[NH_4^+]/[SO_4^{2-}]$ ratio higher than 1, compared to 36.8% at night, suggesting that $SO_4^{2-}$ was not completely neutralized by $NH_4^+$ or that there was not enough $NH_4^+$ to neutralize $H_2SO_4$ in coarse mode (Figs. S3a, c). In this case, the formation of coarse $SO_4^{2-}$ could be explained by the reaction of $SO_2$ or $H_2SO_4$ with pre-existing $Ca^{2+}$ and/or $Na^+$ particles. In addition, almost all samples had $[NH_4^+]/([SO_4^{2-}] + [NO_3^-])$ ratios that were lower than 1 in coarse mode during the day (96.2%) and at night (100%), suggesting that not all $NO_3^-$ was neutralized by $NH_4^+$ (Figs. S3b, d). These results indicate that these samples were ammonium-poor and that the aerosols were acidic. As mentioned in Section 3.1.2, coarse $NO_3^-$ can arise from heterogeneous reactions between $HNO_3$ and/or gaseous precursors of $NO_3^-$ and sea salts or crustal species. Thus, the formation pathway for $NO_3^-$ in coarse mode can be examined further. Under the assumption that $SO_4^{2-}$ is preferably neutralized by $NH_4^+$ compared to $NO_3^-$, excess $[NO_3^-]$ can be calculated using Eq. (3):

$$\text{Excess } [NO_3^-] = [NO_3^-] - [NH_4^+] - [SO_4^{2-}] \quad (3)$$

The strong correlation between excess $[NO_3^-]$ and $Ca^{2+}$ and/or $Mg^{2+}$ except in January (Fig. S4) indicates the presence of $Mg(NO_3)_2$ and/or $Ca(NO_3)_2$ in coarse particles, which might explain the formation of coarse $NO_3^-$ in this study (Dasch and Cadle 1990; Pakkanen et al. 1996; Wolff 1984). This result is consistent with previous research conducted on Jeju Island, South Korea (Park et al. 2004).

Fig. S5 presents scatter plots of the mole charge ratio of $[NH_4^+]$ to $[SO_4^{2-}]$ and to $[SO_4^{2-}]$ + $[NO_3^-]$ in fine mode during the sampling period. In general, a similar formation mechanism during the day and at night was observed. Almost all of the $[NH_4^+]/[SO_4^{2-}]$ ratios were higher than 1 (Figs. S5a, c), suggesting that these samples were ammonium-rich (Squizzato et al. 2013). In this case, two moles of $NH_4^+$ are removed by one mole of $SO_4^{2-}$, meaning that $SO_4^{2-}$ is completely neutralized by $NH_4^+$ to produce $(NH_4)_2SO_4$. The mole charge ratio of $[NH_4^+]$ to $[SO_4^{2-}]$ + $[NO_3^-]$ is used to determine aerosol acidity. An aerosol is considered acidic if the ratio of $[NH_4^+]$ to $[SO_4^{2-}]$ + $[NO_3^-]$ is close to 1 and alkaline if it is greater than 1 (Li et al. 2014; Meng et al. 2016). In this study, almost all of the samples had mole ratios of $[NH_4^+]$ to $[SO_4^{2-}]$ + $[NO_3^-]$ that were higher than 1, indicating that the aerosols were alkaline and that almost all $NO_3^-$ could be neutralized by $NH_4^+$ (Figs. S5b, d). In the ammonium-poor samples ($[NH_4^+]/([SO_4^{2-}] + [NO_3^-]) < 1$), $SO_4^{2-}$ is mainly neutralized by $NH_4^+$ to form $NH_4HSO_4$, suggesting that $SO_4^{2-}$ is not completely neutralized by $NH_4^+$ (Li et al. 2014).

To better understand $NH_4NO_3$ formation, the $[NO_3^-]/[SO_4^{2-}]$ ratio as a function of the normalized $NH_4^+$ concentration (i.e., the $[NH_4^+]/[SO_4^{2-}]$ molar ratio) is presented in Figs. S6a, c. Because of the clear change in the slope observed at a $[NH_4^+]/[SO_4^{2-}]$ molar ratio of 1.5, this was used as the threshold in the present study to define ammonium-rich (i.e., $[NH_4^+]/[SO_4^{2-}] > 1.5$) samples (Arsene et al. 2011; Huang et al. 2011; Pathak et al. 2009b), in which $NO_3^-$ is stabilized by $NH_4^+$. In comparison, in ammonium-poor samples (i.e., $[NH_4^+]/[SO_4^{2-}] < 1.5$), $NO_3^-$ formation is driven by the (a) homogeneous gas-phase reaction of $HNO_3$ and $NH_3$ and sea salts or fine crustal species and (b) heterogeneous hydrolysis of $N_2O_5$ on the wet surface of pre-existing aerosols (Zhao and Gao 2008). Previous studies have indicated that a normalized $NH_4^+$ concentration of 1.5 may be a fixed limit for excess ammonium, as shown in Eq. (4):

$$\text{Excess } [NH_4^+] = ([NH_4^+]/[SO_4^{2-}] - 1.5) \times [SO_4^{2-}] \quad (4)$$

In this study, as seen in the plot of the mole charge ratio of $NO_3^-$ as a function of excess $[NH_4^+]$, the concentration of $NO_3^-$ rose as the levels of excess $[NH_4^+]$ increased in ammonium-rich samples, indicating that the homogeneous reaction of $HNO_3$ and $NH_3$ plays a crucial role in the formation of fine particulate $NO_3^-$ (Figs. S6b, d). In contrast, the formation of $NO_3^-$ in ammonium-poor samples may not be explained by this homogeneous gas-phase reaction, but rather by crustal species in fine mode and the night-time heterogeneous hydrolysis of $N_2O_5$ on the wet surface of pre-existing aerosols (Pathak et al. 2009a). These results indicate that $NH_4^+$ plays a significant role in the formation and size distribution of SIA components in fine particles.

### 3.3.2. Magnesium, calcium, and potassium

$Ca^{2+}$ and $Mg^{2+}$ exhibited a similar unimodal distribution, accumulating at a size of around 1.8–5.6 μm, which agrees with most published studies (Park and Lee 2015; Park et al. 2019; Park et al. 2004). In the atmosphere, these species are believed to mostly derive from natural sources (e.g., soil particles or falling dust), with minor contributions from sea salts. Many published studies have reported extremely high $PM_{10}$ concentrations in spring because of the influence of large particles in dust storms arriving in Korea from the deserts of China and Mongolia (Chung 1992; In and Park 2002; Kim and Park 2001). Therefore, the air quality in South Korea in spring might be greatly affected by dust storms, and further in-depth investigation is essential. According to a report from the KMA, South Korea experienced two Asian dust events on April 05–06, 2019, which led to increased levels of coarse particles in the days following due to dust being blown

from the ground into the atmosphere. This could account for the high concentrations of $Mg^{2+}$ and $Ca^{2+}$ in April. In addition, sea-salt particles, which are enhanced by the prevailing northeasterly winds in September, could be a source contributor to $Mg^{2+}$ in coarse mode (Zhang et al. 2018; Zhao et al. 2011) due to the geographical position of this study area. As discussed in the previous section, $Mg^{2+}$ played an important role in the formation of coarse $NO_3^-$ in this study, and thus it could explain for the peak of $Mg^{2+}$ in September.

A bimodal distribution for $K^+$ was found, with both coarse and fine peaks. $K^+$ has been reported to derive from multiple sources, such as vegetation, soils, sea salts, coal combustion, and the burning of biomass (e.g., forest fires and bio-fuel consumption), with the fine mode peak possibly related to the burning of biomass and coal combustion, and the coarse peak arising from sea salts and/or dust sources (Li et al. 2013; Zhang et al. 2018). In addition, long-range atmospheric transport from the neighboring countries affects the air quality in South Korea during the cold periods (Thang et al. 2020; Vuong et al. 2020). Thus, the higher concentrations of fine $K^+$ in January and November than in other months may be a consequence of coal and/or biomass combustion transported from the outside of Ulsan by prevailing northwesterly winds.

### 3.3.3. Sodium, chloride, and fluoride

It is obvious that the ocean was the main source of $Na^+$ and $Cl^-$ in the aerosols. We found that $Na^+$ and $Cl^-$ both had bimodal distributions in January, while a single peak in coarse mode was observed in the other months. Fig. S7 shows that $Na^+$ always had a very strong correlation with $Cl^-$ in coarse mode except in January, which is indicative of the influence of the East Sea, with most $Na^+$ and $Cl^-$ present as NaCl in coarse particles in April, September, and November. Coarse $Cl^-$ mainly derives from sea spray, while fine $Cl^-$ originates from coal combustion (Sun et al. 2006). This could explain the small peak in fine $Cl^-$ in January, which might be related to coal combustion for heating in the areas surrounding Ulsan, especially at night.

Despite being very harmful to the health, there have been very few studies to date focusing on $F^-$ because of its very low concentration in the atmosphere (Zhang et al. 2018). In this study, $F^-$ was only found in January, peaking at 0.32–0.56 and 3.2–10 μm in fine and coarse mode, respectively, with a relatively low concentration in April. The $F^-$ in fine particles mainly arises from photochemical reactions on the surface of particles, while the $F^-$ in coarse particles may derive from the decomposition of living organisms and soil (Xiu et al. 2004; Zhang et al. 2018)

## 4. Summary and conclusion

A comprehensive analysis of WSIIs in 11 size classes of PM was conducted to investigate day–night differences and size distributions at a semi-rural site in Ulsan, South Korea. Monthly variation in individual WSIIs was evident, which is likely due to the differences in meteorology, chemistry, and source contributors throughout the four-month field campaign. The highest level of fine $SO_4^{2-}$ in April (2.19 μg/m$^3$) was likely due to the high loading of $SO_2$ emitted from industrial areas and carried to the site on the prevailing southeasterly winds during this month, with the $SO_2$ converted into $SO_4^{2-}$ under strong solar radiation and high temperatures. Fine $NO_3^-$ and $NH_4^+$ were highest in January and lowest in September, which could be explained by their negative correlation with temperature. $NO_3^-$ was not only the dominant contributor to fine particles but was also one of the most abundant species detected within coarse particles. This may be the result of reactions involving the gaseous precursors of $NO_3^-$ or $HNO_3$ and sea salts, which is expected to be the dominant species in coarse particles in a coastal city such as Ulsan. $Na^+$, $Cl^-$, and $Ca^{2+}$ were the largest contributors (~70%) to total WSIIs in coarse particles, deriving mainly from sea salts, falling dust, and soil particles.

The calculated COD was lower than 0.27 for both coarse and fine PM over the four months, while the CODs of individual WSIIs varied, indicating significant differences in meteorology, chemistry, and sources between day and night. The CODs of coarse $NO_3^-$, $Na^+$ and $Cl^-$ were higher than 0.27 in April and/or September, with a higher average concentration during the day than at night, illustrating the strong influence of the southeasterly winds in April and the northeasterly winds in September during the day arising from sea-breeze circulation. In fine mode, the CODs for $SO_4^{2-}$ were always higher than 0.27, highlighting the importance of meteorology during the day and at night to the source contribution of the gaseous precursors of $SO_4^{2-}$ over the sampling period. $NO_3^-$ and $NH_4^+$ levels were associated with the temperature-dependent equilibrium of $NH_4NO_3$ with a COD lower than 0.27 in January and a higher average level at night than during the day in other months.

The size distributions of $Na^+$, $K^+$, $F^-$, $Cl^-$, $NO_3^-$, and $SO_4^{2-}$ were bimodal, with fine particles peaking at 0.18–0.56 μm and coarse particles peaking at 1.8–5.6 μm. $NH_4^+$ was mainly found within the 0.18–0.56 μm size range, thus exhibiting a unimodal distribution in fine mode, while both $Mg^{2+}$ and $Ca^{2+}$ had a unimodal peak in coarse mode at 1.8–5.6 μm. We also found that $NO_3^-$ was mainly generated from the heterogeneous reaction of $HNO_3$ or gaseous precursors of $NO_3^-$ with sea salts or crustal species on pre-existing coarse particles, while the homogeneous reaction between $HNO_3$ and $NH_3$ was dominant in the generation of fine $NO_3^-$ in Ulsan.

Although a significant difference in the concentration and size distribution of WSIIs was observed in the present study, their formation pathways were similar between day and night, especially for SNA. Therefore, to reduce PM pollution episodes due to secondary formation in Ulsan, a reduction in the emission of the gaseous precursors (i.e., $SO_2$, $NO_x$, and $NH_3$) of SIA components is necessary. This study also clarifies the influence of meteorological conditions on day–night variation in WSIIs in both coarse and fine particles. Furthermore, it provides an in-depth insight into the formation mechanisms for atmospheric aerosols at a semi-rural site in a multi-industrial city, and the results of this study can be used as the foundation for further studies in urban and industrial areas.

## Declaration of Competing Interest

None.

## Acknowledgements

This study was supported by the National Research Foundation of Korea (NRF) grant funded by the Korean Government (MEST) (2020R1A2B5B01002669) and the 2020 Research Fund (1.200044) of the Ulsan National Institute of Science and Technology (UNIST). In addition, this work was partially supported by the Rural Development Administration of Korea (PJ014297).

**CRediT authorship contribution statement.**

**Tien Van Do:** Writing – original draft.

**Quang Tran Vuong:** Formal analysis.

**Sung-Deuk Choi:** Supervision, Project administration.

Declaration of interest: None

## Appendix A. Supplementary data

Supplementary data to this article can be found online at https://doi.org/10.1016/j.atmosres.2020.105145.

## References

Ali-Mohamed, A.Y., 1991. Estimation of inorganic particulate matter in the atmosphere of Isa Town, Bahrain, by dry deposition. Atmos. Environ. 25, 397–405.

Arsene, C., Olariu, R.I., Zarmpas, P., Kanakidou, M., Mihalopoulos, N., 2011. Ion composition of coarse and fine particles in Iasi, North-Eastern Romania: Implications for

aerosols chemistry in the area. Atmos. Environ. 45, 906–916.
Byun, S.-J., Choi, K.-C., 2019. Chemical composition and size distribution of aerosol particle in high polluted periods. Asian Journal of Atmospheric Environment 13, 233–239.
Cabada, J.C., Rees, S., Takahama, S., Khlystov, A., Pandis, S.N., Davidson, C.I., Robinson, A.L., 2004. Mass size distributions and size resolved chemical composition of fine particulate matter at the Pittsburgh supersite. Atmos. Environ. 38, 3127–3141.
Chan, C.K., Yao, X., 2008. Air pollution in mega cities in China. Atmos. Environ. 42, 1–42.
Chandra, S., Kulshrestha, M.J., Kumar, B., Kotnala, R.K., 2019. Investigating daytime and night-time differences with the seasonal trend and sources of inorganic fine aerosols in Indo-Gangetic plain. Journal of Earth System Science 128, 40.
Chung, Y.-S., 1992. On the observations of yellow sand (dust storms) in Korea. Atmos. Environ. 26, 2743–2749.
Clarke, K., Kwon, H.-O., Choi, S.-D., 2014. Fast and reliable source identification of criteria air pollutants in an industrial city. Atmos. Environ. 95, 239–248.
Contini, D., Cesari, D., Genga, A., Siciliano, M., Ielpo, P., Guascito, M.R., Conte, M., 2014. Source apportionment of size-segregated atmospheric particles based on the major water-soluble components in Lecce (Italy). Sci. Total Environ. 472, 248–261.
Dasch, J.M., Cadle, S.H., 1990. The removal of nitric acid to atmospheric particles during a wintertime field study. Atmos. Environ. Part A 24, 2557–2562.
Deshmukh, D.K., Tsai, Y.I., Deb, M.K., Zarmpas, P., 2012. Characteristics and sources of water-soluble ionic species associated with PM10 particles in the ambient air of Central India. Bull. Environ. Contam. Toxicol. 89, 1091–1097.
Eldering, A., Solomon, P.A., Salmon, L.G., Fall, T., Cass, G.R., 1991. Hydrochloric acid: a regional perspective on concentrations and formation in the atmosphere of Southern California. Atmos. Environ. 25, 2091–2102.
Feng, Y., Penner, J.E., 2007. Global modeling of nitrate and ammonium: Interaction of aerosols and tropospheric chemistry. Journal of Geophysical Research: Atmospheres 112.
Galindo, N., Yubero, E., 2017. Day-night variability of water-soluble ions in PM10 samples collected at a traffic site in southeastern Spain. Environ. Sci. Pollut. Res. 24, 805–812.
Guo, S., Hu, M., Zamora, M.L., Peng, J., Shang, D., Zheng, J., Du, Z., Wu, Z., Shao, M., Zeng, L., Molina, M.J., Zhang, R., 2014. Elucidating severe urban haze formation in China. Proc. Natl. Acad. Sci. 111, 17373.
Hu, M., Wu, Z., Slanina, J., Lin, P., Liu, S., Zeng, L., 2008. Acidic gases, ammonia and water-soluble ions in PM2.5 at a coastal site in the Pearl River Delta, China. Atmos. Environ. 42, 6310–6320.
Huang, X., Qiu, R., Chan, C.K., Ravi Kant, P., 2011. Evidence of high PM2.5 strong acidity in ammonia-rich atmosphere of Guangzhou, China: transition in pathways of ambient ammonia to form aerosol ammonium at [NH4+]/[SO42–]=1.5. Atmos. Res. 99, 488–495.
Huang, R.-J., Zhang, Y., Bozzetti, C., Ho, K.-F., Cao, J.-J., Han, Y., Daellenbach, K.R., Slowik, J.G., Platt, S.M., Canonaco, F., Zotter, P., Wolf, R., Pieber, S.M., Bruns, E.A., Crippa, M., Ciarelli, G., Piazzalunga, A., Schwikowski, M., Abbaszade, G., Schnelle-Kreis, J., Zimmermann, R., An, Z., Szidat, S., Baltensperger, U., Haddad, I.E., Prévôt, A.S.H., 2014. High secondary aerosol contribution to particulate pollution during haze events in China. Nature 514, 218.
Huang, X., Liu, Z., Zhang, J., Wen, T., Ji, D., Wang, Y., 2016. Seasonal variation and secondary formation of size-segregated aerosol water-soluble inorganic ions during pollution episodes in Beijing. Atmos. Res. 168, 70–79.
In, H.-J., Park, S.-U., 2002. A simulation of long-range transport of Yellow sand observed in April 1998 in Korea. Atmos. Environ. 36, 4173–4187.
Kadowaki, S., 1976. Size distribution of atmospheric total aerosols, sulfate, ammonium and nitrate particulates in the Nagoya area. Atmos. Environ. 10, 39–43.
Kang, H., Zhu, B., Su, J., Wang, H., Zhang, Q., Wang, F., 2013. Analysis of a long-lasting haze episode in Nanjing, China. Atmos. Res. 120-121, 78–87.
Kawamura, K., Narukawa, M., Li, S.M., Barrie, L.A., 2007. Size distributions of dicarboxylic acids and inorganic ions in atmospheric aerosols collected during polar sunrise in the Canadian high Arctic. J. Geophys. Res.-Atmos. 112 (12).
Kim, B.-G., Park, S.-U., 2001. Transport and evolution of a winter-time Yellow sand observed in Korea. Atmos. Environ. 35, 3191–3201.
Kim, Y.P., Lee, J.H., Baik, N.J., Kim, J.Y., Shim, S.-G., Kang, C.-H., 1998. Summertime characteristics of aerosol composition at Cheju Island, Korea. Atmos. Environ. 32, 3905–3915.
Kim, K.-H., Mishra, V.K., Kang, C.-H., Choi, K.C., Kim, Y.J., Kim, D.S., 2006. The ionic compositions of fine and coarse particle fractions in the two urban areas of Korea. J. Environ. Manag. 78, 170–182.
Kleeman, M.J., Schauer, J.J., Cass, G.R., 1999. Size and composition distribution of fine particulate matter emitted from wood burning, meat charbroiling, and cigarettes. Environmental Science & Technology 33, 3516–3523.
Kwon, H.-O., Park, M.-K., Kim, S.-J., Choi, J., Oh, J., Ahn, J.-Y., Choi, S.-D., 2019. Size distributions of atmospheric particulate matter and associated trace metals in the multi-industrial city of Ulsan, Korea. Environmental Engineering Research 24, 331–338.
Lee, T., Choi, J., Lee, G., Ahn, J., Park, J.S., Atwood, S.A., Schurman, M., Choi, Y., Chung, Y., Collett, J.L., 2015. Characterization of aerosol composition, concentrations, and sources at Baengnyeong Island, Korea using an aerosol mass spectrometer. Atmos. Environ. 120, 297–306.
Li, X., Wang, L., Ji, D., Wen, T., Pan, Y., Sun, Y., Wang, Y., 2013. Characterization of the size-segregated water-soluble inorganic ions in the Jing-Jin-Ji urban agglomeration: Spatial/temporal variability, size distribution and sources. Atmos. Environ. 77, 250–259.
Li, L., Yin, Y., Kong, S., Wen, B., Chen, K., Yuan, L., Li, Q., 2014. Altitudinal effect to the size distribution of water soluble inorganic ions in PM at Huangshan, China. Atmos. Environ. 98, 242–252.
Liu, S., Hu, M., Slanina, S., He, L.-Y., Niu, Y.-W., Bruegemann, E., Gnauk, T., Herrmann, H., 2008. Size distribution and source analysis of ionic compositions of aerosols in polluted periods at Xinken in Pearl River Delta (PRD) of China. Atmos. Environ. 42, 6284–6295.
Liu, Z., Gao, W., Yu, Y., Hu, B., Xin, J., Sun, Y., Wang, L., Wang, G., Bi, X., Zhang, G., Xu, H., Cong, Z., He, J., Xu, J., Wang, Y., 2018. Characteristics of PM2.5 mass concentrations and chemical species in urban and background areas of China: emerging results from the CARE-China network. Atmos. Chem. Phys. 18, 8849–8871.
Matsuki, A., Iwasaka, Y., Shi, G., Zhang, D., Trochkine, D., Yamada, M., Kim, Y.-S., Chen, B., Nagatani, T., Miyazawa, T., Nagatani, M., Nakata, H., 2005. Morphological and chemical modification of mineral dust: Observational insight into the heterogeneous uptake of acidic gases. Geophys. Res. Lett. 32.
Matsumoto, M., Okita, T., 1998. Long term measurements of atmospheric gaseous and aerosol species using an annular denuder system in Nara, Japan. Atmos. Environ. 32, 1419–1425.
Meng, C.C., Wang, L.T., Zhang, F.F., Wei, Z., Ma, S.M., Ma, X., Yang, J., 2016. Characteristics of concentrations and water-soluble inorganic ions in PM2.5 in Handan City, Hebei province, China. Atmos. Res. 171, 133–146.
Mozurkewich, M., 1993. The dissociation constant of ammonium nitrate and its dependence on temperature, relative humidity and particle size. Atmos. Environ. 27, 261–270.
Nicolás, J.F., Galindo, N., Yubero, E., Pastor, C., Esclapez, R., Crespo, J., 2009. Aerosol inorganic ions in a semiarid region on the Southeastern Spanish mediterranean coast. Water Air Soil Pollut. 201, 149–159.
Ocskay, R., Salma, I., Wang, W., Maenhaut, W., 2006. Characterization and diurnal variation of size-resolved inorganic water-soluble ions at a rural background site. J. Environ. Monit. 8, 300–306.
Pakkanen, T.A., 1996. Study of formation of coarse particle nitrate aerosol. Atmos. Environ. 30, 2475–2482.
Pakkanen, T.A., Kerminen, V.-M., Hillamo, R.E., Màkinen, M., Màkelà, T., Virkkula, A., 1996. Distribution of nitrate over sea-salt and soil derived particles-Implications from a field study. J. Atmos. Chem. 24, 189–205.
Park, G.-h., Lee, B.-k., 2015. Size distribution characteristics of water-soluble ionic components in airborne particulate matter in Busan. Journal of Korean Society for Atmospheric Environment 31, 287–301.
Park, S.H., Song, C.B., Kim, M.C., Kwon, S.B., Lee, K.W., 2004. Study on size distribution of total aerosol and water-soluble ions during an asian dust storm event at Jeju island, Korea. Environ. Monit. Assess. 93, 157–183.
Park, S.-S., Cho, S.-Y., Jung, C.-H., Lee, K.-H., 2016. Characteristics of water-soluble inorganic species in PM10 and PM2.5 at two coastal sites during spring in Korea. Atmospheric Pollution Research 7, 370–383.
Park, M.-K., Kim, S.-J., Song, S.-A., Kwon, H.-O., Choi, S.-D., 2019. Size distributions of airborne particulate matter associated ions and their pollution sources in Ulsan, Korea. Journal of the Korean Society for Environmental Analysis 22, 1–9.
Pathak, R.K., Wu, W.S., Wang, T., 2009a. Summertime PM2.5 ionic species in four major cities of China: nitrate formation in an ammonia-deficient atmosphere. Atmos. Chem. Phys. 9, 1711–1722.
Pathak, R.K., Wu, W.S., Wang, T., 2009b. Summertime PM2.5 ionic species in four major cities of China: nitrate formation in an ammonia-deficient atmosphere. Atmos. Chem. Phys. 9, 1711–1722.
Pio, C.A., Harrison, R.M., 1987. Vapour pressure of ammonium chloride aerosol: effect of temperature and humidity. Atmos. Environ. 21, 2711–2715.
Querol, X., Alastuey, A., Viana, M.M., Rodriguez, S., Artiñano, B., Salvador, P., Garcia do Santos, S., Fernandez Patier, R., Ruiz, C.R., de la Rosa, J., Sanchez de la Campa, A., Menendez, M., Gil, J.I., 2004. Speciation and origin of PM10 and PM2.5 in Spain. J. Aerosol Sci. 35, 1151–1172.
Salvador, P., Artinano, B., Alonso, D.G., Querol, X., Alastuey, A., 2004a. Identification and characterisation of sources of PM10 in Madrid (Spain) by statistical methods. Atmos. Environ. 38, 435–447.
Salvador, P., Artíñano, B., Alonso, D.G., Querol, X., Alastuey, A., 2004b. Identification and characterisation of sources of PM10 in Madrid (Spain) by statistical methods. Atmos. Environ. 38, 435–447.
Shi, Y., Chen, J., Hu, D., Wang, L., Yang, X., Wang, X., 2014. Airborne submicron particulate (PM1) pollution in Shanghai, China: Chemical variability, formation/dissociation of associated semi-volatile components and the impacts on visibility. Sci. Total Environ. 473-474, 199–206.
Shon, Z.-H., Kim, K.-H., Song, S.-K., Jung, K., Kim, N.-J., Lee, J.-B., 2012. Relationship between water-soluble ions in PM2.5 and their precursor gases in Seoul megacity. Atmos. Environ. 59, 540–550.
Sievering, H., Gorman, E., Ley, T., Pszenny, A., Springer-Young, M., Boatman, J., Kim, Y., Nagamoto, C., Wellman, D., 1995. Ozone oxidation of sulfur in sea-salt aerosol particles during the Azores marine aerosol and gas exchange experiment. Journal of Geophysical Research: Atmospheres 100, 23075–23081.
Song, J.-M., Bu, J.-O., Lee, J.-Y., Kim, W.-H., Kang, C.-H., 2017. Ionic compositions of PM10 and PM2.5 related to meteorological conditions at the Gosan site, Jeju island from 2013 to 2015. Asian Journal of Atmospheric Environment 11, 313–321.
Squizzato, S., Masiol, M., Brunelli, A., Pistollato, S., Tarabotti, E., Rampazzo, G., Pavoni, B., 2013. Factors determining the formation of secondary inorganic aerosol: a case study in the Po Valley (Italy). Atmos. Chem. Phys. 13, 1927–1939.
Stockwell, W.R., Watson, J.G., Robinson, N.F., Steiner, W., Sylte, W.W., 2000. The ammonium nitrate particle equivalent of NOx emissions for wintertime conditions in Central California's San Joaquin Valley. Atmos. Environ. 34, 4711–4717.
Stockwell, W.R., Kuhns, H., Etyemezian, V., Green, M.C., Chow, J.C., Watson, J.G., 2003. The Treasure Valley secondary aerosol study II: modeling of the formation of inorganic secondary aerosols and precursors for southwestern Idaho. Atmos. Environ. 37, 525–534.

Sudheer, A.K., Rengarajan, R., Deka, D., Bhushan, R., Singh, S.K., Aslam, M.Y., 2014. Diurnal and seasonal characteristics of aerosol ionic constituents over an urban location in western India: secondary aerosol formation and meteorological influence. Aerosol Air Qual. Res. 14, 1701–1713.

Sun, Y., Zhuang, G., Wang, Y., Han, L., Guo, J., Dan, M., Zhang, W., Wang, Z., Hao, Z., 2004. The air-borne particulate pollution in Beijing: concentration, composition, distribution and sources. Atmos. Environ. 38, 5991–6004.

Sun, Y., Zhuang, G., Tang, A., Wang, Y., An, Z., 2006. Chemical characteristics of PM2.5 and PM10 in haze−fog episodes in Beijing. Environmental Science & Technology 40, 3148–3155.

Sun, Z., Mu, Y., Liu, Y., Shao, L., 2013. A comparison study on airborne particles during haze days and non-haze days in Beijing. Sci. Total Environ. 456-457, 1–8.

Thang, P.Q., Kim, S.-J., Lee, S.-J., Kim, C.H., Lim, H.-J., Lee, S.-B., Kim, J.Y., Vuong, Q.T., Choi, S.-D., 2020. Monitoring of polycyclic aromatic hydrocarbons using passive air samplers in Seoul, South Korea: Spatial distribution, seasonal variation, and source identification. Atmos. Environ. 229, 117460.

Tian, M., Wang, H., Chen, Y., Yang, F., Zhang, X., Zou, Q., Zhang, R., Ma, Y., He, K., 2016. Characteristics of aerosol pollution during heavy haze events in Suzhou, China. Atmos. Chem. Phys. 16, 7357–7371.

Tie, X., Cao, J., 2009. Aerosol pollution in China: present and future impact on environment. Particuology 7, 426–431.

Vuong, Q.T., Thang, P.Q., Nguyen, T.N.T., Ohura, T., Choi, S.-D., 2020. Seasonal variation and gas/particle partitioning of atmospheric halogenated polycyclic aromatic hydrocarbons and the effects of meteorological conditions in Ulsan, South Korea. Environ. Pollut. 263, 114592.

Walker, J.T., Robarge, W.P., Shendrikar, A., Kimball, H., 2006. Inorganic PM2.5 at a U.S. agricultural site. Environ. Pollut. 139, 258–271.

Wang, Y., Zhuang, G., Tang, A., Yuan, H., Sun, Y., Chen, S., Zheng, A., 2005. The ion chemistry and the source of PM2.5 aerosol in Beijing. Atmos. Environ. 39, 3771–3784.

Wilson, J.G., Kingham, S., Pearce, J., Sturman, A.P., 2005. A review of intraurban variations in particulate air pollution: Implications for epidemiological research. Atmos. Environ. 39, 6444–6462.

Wolff, G.T., 1984. On the nature of nitrate in coarse continental aerosols. Atmos. Environ. 18, 977–981.

Wongphatarakul, V., Friedlander, S.K., Pinto, J.P., 1998. A comparative study of PM2.5 ambient aerosol chemical databases. Environmental Science & Technology 32, 3926–3934.

Wu, Z., Hu, M., Shao, K., Slanina, J., 2009. Acidic gases, NH3 and secondary inorganic ions in PM10 during summertime in Beijing, China and their relation to air mass history. Chemosphere 76, 1028–1035.

Xing, X., Chen, Z., Tian, Q., Mao, Y., Liu, W., Shi, M., Cheng, C., Hu, T., Zhu, G., Li, Y., Zheng, H., Zhang, J., Kong, S., Qi, S., 2020. Characterization and source identification of PM2.5-bound polycyclic aromatic hydrocarbons in urban, suburban, and rural ambient air, Central China during summer harvest. Ecotoxicol. Environ. Saf. 191, 110219.

Xiu, G., Zhang, D., Chen, J., Huang, X., Chen, Z., Guo, H., Pan, J., 2004. Characterization of major water-soluble inorganic ions in size-fractionated particulate matters in Shanghai campus ambient air. Atmos. Environ. 38, 227–236.

Xu, M., Sbihi, H., Pan, X., Brauer, M., 2020. Modifiers of the effect of short-term variation in PM2.5 on mortality in Beijing, China. Environ. Res. 183, 109066.

Yamasoe, M.A., Artaxo, P., Miguel, A.H., Allen, A.G., 2000. Chemical composition of aerosol particles from direct emissions of vegetation fires in the Amazon Basin: water-soluble species and trace elements. Atmos. Environ. 34, 1641–1653.

Yang, F., Ye, B., He, K., Ma, Y., Cadle, S.H., Chan, T., Mulawa, P.A., 2005. Characterization of atmospheric mineral components of PM2.5 in Beijing and Shanghai, China. Sci. Total Environ. 343, 221–230.

Yoshizumi, K., Hoshi, A., 1985. Size distributions of ammonium nitrate and sodium nitrate in atmospheric aerosols. Environmental Science & Technology 19, 258–261.

Yudovich, Y., Ketris, M., 2006. Chlorine in coal: a review. International Journal of Coal Geology - INT J COAL GEOL 67, 127–144.

Zhang, L., Vet, R., Wiebe, A., Mihele, C., Sukloff, B., Chan, E., Moran, M.D., Iqbal, S., 2008. Characterization of the size-segregated water-soluble inorganic ions at eight Canadian rural sites. Atmos. Chem. Phys. 8, 7133–7151.

Zhang, R., Wang, G., Guo, S., Zamora, M.L., Ying, Q., Lin, Y., Wang, W., Hu, M., Wang, Y., 2015. Formation of urban fine particulate matter. Chem. Rev. 115, 3803–3855.

Zhang, J., Tong, L., Huang, Z., Zhang, H., He, M., Dai, X., Zheng, J., Xiao, H., 2018. Seasonal variation and size distributions of water-soluble inorganic ions and carbonaceous aerosols at a coastal site in Ningbo, China. Sci. Total Environ. 639, 793–803.

Zhao, Y., Gao, Y., 2008. Mass size distributions of water-soluble inorganic and organic ions in size-segregated aerosols over metropolitan Newark in the US east coast. Atmos. Environ. 42, 4063–4078.

Zhao, J., Zhang, F., Xu, Y., Chen, J., 2011. Characterization of water-soluble inorganic ions in size-segregated aerosols in coastal city, Xiamen. Atmos. Res. 99, 546–562.

Zhou, J., Xing, Z., Deng, J., Du, K., 2016. Characterizing and sourcing ambient PM2.5 over key emission regions in China I: Water-soluble ions and carbonaceous fractions. Atmos. Environ. 135, 20–30.